Applied Catalysis B: Environmental 255 (2019) 117740

Contents lists available at ScienceDirect

Applied Catalysis B: Environmental

journal homepage: www.elsevier.com/locate/apcatb

Chitosan functionalized activated coke for Au nanoparticles anchoring: Green synthesis and catalytic activities in hydrogenation of nitrophenols and azo dyes

Yukui Fu[a,b,1], Lei Qin[a,b,1], Danlian Huang[a,b,1], Guangming Zeng[a,b,*], Cui Lai[a,b,*], Bisheng Li[a,b], Jiangfan He[a,b], Huan Yi[a,b], Mingming Zhang[a,b], Min Cheng[a,b], Xiaofeng Wen[a,b]

[a] College of Environmental Science and Engineering, Hunan University, Changsha, 410082, PR China
[b] Key Laboratory of Environmental Biology and Pollution Control, Hunan University, Ministry of Education, PR China

ARTICLE INFO

Keywords:
Activated coke
Chitosan
Au nanoparticles
Nitrophenols
Catalytic hydrogenation

ABSTRACT

Herein, chitosan (CTS) functionalized activated coke (AC) is proposed as an excellent platform for Au nanoparticles (NPs) anchoring. Due to the surface-rich hydroxyl and amino groups, CTS can act as a three-functional agent such as reductant, linker and stabilizer to improve the stability of catalysts and realize a green synthesis without adding any additional chemicals. The Au NPs/CTS/AC catalysts exhibited a high catalytic activity in hydrogenation of 4-nitrophenol with the rate constant k_{app} of 0.6994 min^{-1} and turnover frequency (TOF) of 202 h^{-1}. Several effect parameters: Au loading amount, environmental water samples and common anions were discussed in detail. Besides, the pH and dissolved oxygen (DO) in different environmental water were measured. The results show that although the catalytic performance of Au NPs/CTS/AC was inhibited in some extent, it could maintain a relatively high catalytic activity in real water samples. In addition, the as-prepared catalysts also displayed high catalytic activity in the hydrogenation of various different substituent nitrophenols and azo dyes, indicating the generality of catalysts, and showed good recyclability with the catalytic performance remained 90% within 7 min 40 s over six recycles. The mechanism of green synthetic pathway and catalytic hydrogenation of nitrophenols over Au NPs/CTS/AC was proposed. The results demonstrated that the Au NPs could facilitate Au-H intermediates to form and thus enhance the catalytic activity. This green synthetic Au NPs/CTS/AC has been proved to be a viable and potential material for environmental pollution treatment of nitrophenols and azo dyes hydrogenation.

1. Introduction

Owing to the unique structure and high activity, metal catalysts dispersed on solid supports dominate the technology of hydrogenation, hydrogenolysis, oxidation, coupling reaction and so on [1–4]. They are the keys to environmental protection by elimination and conversion of pollutants in atmosphere and water [5–7]. Gold nanoparticles (Au NPs) catalysts are especially attractive, because they are lower leaching toxicity, mild reaction conditions and high catalytic activity in many reactions compared with other metal NPs [8,9]. However, the self-aggregation of Au NPs with the high surface energy results in a decrement of catalytic activity. Thus, Au NPs dispersedly anchored on a rational support can efficiently inhibit the aggregation and thus enhance the catalytic activity.

Among numerous materials, carbon-based supports such as graphene, mesoporous carbon, carbon nanotube, and carbon nitride have offered a number of advantages over other supports (e.g. metal oxide, silica, polymers) due to their chemical stability and high mechanical strength [10–13]. The carbon-based Au NPs catalysts have been proved to be a relatively high efficient catalyst [14]. But these carbon supports are usually prepared with complex progress, which is relatively expensive [15,16]. Thus, we paid attention to activated coke (AC), a widely available inert support with appreciable environmental and economic benefits [17]. The advantages of AC with respect to other carbon materials involve easier accessibility, easier regeneration and lower cost [18–20]. AC usually consists of more macropore and mesopore but less micropore than activated carbon, which can prevent metal catalysts from jamming and encourage diffusion of aqueous species into

* Corresponding authors at: College of Environmental Science and Engineering, Hunan University, Changsha, 410082, PR China.
E-mail addresses: zgming@hnu.edu.cn (G. Zeng), laicui@hnu.edu.cn (C. Lai).
[1] These authors contribute equally to this article.

https://doi.org/10.1016/j.apcatb.2019.05.042
Received 13 November 2018; Received in revised form 10 May 2019; Accepted 12 May 2019
Available online 12 May 2019
0926-3373/

the solid phase [21,22]. Besides, AC possesses graphite-similar layer structure and consists of fused six-membered polyaromatics ting system, which endows it adsorption ability through π-π stacking interaction. AC has been proved to be a suitable material in wastewater treatment [17]. However, the interaction is weak between the inert carbon matrix and Au NPs, resulting in that the inert carbon matrix cannot anchor Au NPs firmly and shedding of active sites [23]. This shortcoming could be overcome by decorating polymers onto the surface of AC. Meanwhile, as the emphasis of technology is gradually shifting towards green synthetic strategy, the utilization of nontoxic, renewable and environmentally benign chemicals are required [24–27]. It is highly desired to find a green synthesis to disperse Au NPs firmly on AC by enhancing their interaction via decorating polymers on AC surface.

Chitosan (CTS) is an attractive natural biopolymer derived from the deacetylation of chitin [28]. This nontoxicity, biocompatibility and polycationic biopolymer makes it appealing for many applications such as drug delivery, metal ion sorption and biodegradable films [29]. Especially, CTS has been widely used to integrate with metal nanoparticles due to the surface-rich hydrophilic groups such as hydroxyl and amino groups and strong macro-chelating ligand [30,31]. These hydrophilic groups are in favor of the reduction, dispersion and stabilization of Au NPs. Thus, the utilize of CTS as a reductant for the formation of Au NPs and a linker between AC and Au NPs is appealing due to its superior properties and surface-rich hydroxyl and amino groups.

Phenolic compounds such as nitrophenols are common toxic and biologically stable organic pollutants in industrial wastewater, and listed by the U.S. EPA as "Priority Pollutants" [32,33]. Azo dyes are extensively used in textile manufacturing and other consuming industries, which are harmful to people's health and environment even at low concentrations [32,34]. As a consequence, searching for an effective and suitable approach for the efficient removal of nitrophenols and azo dyes is extremely essential. It has been well documented that simple hydrogenation of nitrophenols to the corresponding aminophenols could be regarded as the most convenient way to convert organic wastes to value added intermediates. For instance, the produced 4-AP could not only reduce the toxicity, but also serve as available intermediates in numerous medications synthesis and photographic applications [10,32]. Hence, the hydrogenation of nitrophenols with $NaBH_4$ as a hydride source, as well as the hydrogenation of azo dyes, have been investigated in this work.

In this work, we expect to combine CTS with AC and make CTS/AC composite tight interaction with Au NPs to improve the stability of catalysts, and realize the green synthetic process without any additional of toxicity chemicals. The as-prepared Au NPs/CTS/AC was then used for the hydrogenation of 4-NP with $NaBH_4$ as a hydride source. The content of Au can be conveniently controlled by adjusting the addition dosage of $HAuCl_4$. The effects of various environmental water samples (tap water, lake water and river water) with the different pH and DO, and inorganic salt toward 4-NP hydrogenation were taken into consideration on the reaction kinetics. In addition, the catalytic activity of Au NPs/CTS/AC towards nitrophenols hydrogenation (2-NP, 3-NP and 2, 4-DNP) and azo dyes (MO, CR and EBT) were also investigated. Meanwhile, the possible hydrogenation mechanism was proposed for better understanding the Au-mediated hydrogenation of nitrophenols and azo dyes.

2. Experimental

2.1. Materials

Pristine activated coke (AC) was obtained from Clear Science Technology Corporation (China). Chitosan (with 90% degree of deacetylation) was purchased from Pharmacia (Sweden). Analytical grade hydrogen tetrachloroaurate hydrate ($HAuCl_4{\cdot}4H_2O$), sodium borohydride ($NaBH_4$), 2-nitrophenol (2-NP), 3-nitrophenol (3-NP), 4-nitrophenol (4-NP), 2, 4-dinitrophenol (2, 4-DNP), Methyl orange (MO), Congo red (CR) and Erichrome black T (EBT) were purchased from Sinopharm Chemistry Reagent Co., Ltd. (Beijing, China). All chemicals were used without further purification. All solutions were prepared by using ultrapure water (18.25 MΩ cm).

2.2. Synthesis of chitosan functionalized activated coke decorated with Au NPs (denoted as Au NPs/CTS/AC)

CTS/AC: AC was firstly washed by ultrapure water before drying at 60 °C for 12 h under vacuum. Then, the above samples were grinded with ball grinder and sieved to 200 mesh. In a typical procedure, AC (1 g) was first homogenized with 50 mL ultrapure water in ultrasonic bath for 30 min. Then the AC suspension was transferred to a solution contained 500 mg CTS dissolved in 20 mL of 2 wt% acetic acid solution. The mixture solution was under ultrasound for 30 min and then stirred for 24 h. The obtained CTS functionalized AC solution was separated by centrifugation and washed with a large amount of 0.1 M acetic acid solution and ultrapure water to remove unreacted CTS. The final product was dried 24 h at 50 °C under vacuum and denoted as CTS/AC.

Au NPs/CTS/AC: The as-synthesized CTS/AC (200 mg) was dispersed in 60 mL ultrapure water by sonication for 30 min. After that, a certain amount of $HAuCl_4$ solution was added dropwise to aforementioned CTS/AC suspension under stirring with speed of 900 rpm, and then the stirring was continued for another 8 h at 30 °C. The product was collected by centrifugation and thoroughly washed with ultrapure water, followed by drying 24 h at 50 °C under vacuum. A series of Au NPs/CTS/AC catalysts with different Au content were synthesized via similar procedure by varying addition amounts of $HAuCl_4$ (0.35, 0.7, 1.4, 2.8 and 5.6 mL, respectively) and marked as Au NPs/CTS/$AC_{(x)}$ (x = 1, 2, 3, 4, and 5), respectively.

2.3. Characterization

The Fourier transform-infrared spectroscopy (FT-IR) spectra were collected on an 8400 S IRprestige-21 (Shimadzu Corporation, Japan). Transmission electron microscopy (TEM) was conducted to record the morphology of samples (Tecnai G20, USA). Energy dispersive spectroscopy (EDS) was used to determine the element composition. The powder X-Ray diffraction (XRD) spectra were obtained on a 6100 powder diffractometer (Shimadzu Corporation, Japan). Temperature-programmed reduction with a mass spectrometry (H_2-TPR-MS) was conducted on an AutoChem II 2920 (Micromeritics, USA). 100 mg samples were purge treated under a pure He flow (50 mL min^{-1}) at 300 °C for 2 h, and then cooled down to 50 °C and treated under H_2/He mixture (with a ratio of 1:9, 50 mL min^{-1}) for 1 h. Finally, it was heated (10 °C min^{-1}) from room temperature to 800 °C in a flowing H_2/He mixture (with a ratio of 1:9, 50 mL min^{-1}). Meanwhile, the mass spectrometry signals with *m/z* of 30, 44 and 18 were recorded to detect the masses of NO, CO_2 and H_2O molecules, respectively. X-ray photoelectron spectroscopy (XPS) spectra were conducted on Al Kα radiation spectrometer (Thermo Scientific, UK). Inductively coupled plasma atomic emission spectrometry was applied to determine the Au amounts in catalysts (Perkin-Elmer Optima, USA). Zeta potential was measured using a Zeta-sizer Nano-ZS (Malvern). Electron paramagnetic resonance (EPR) spectra were recorded with Bruker EMX-A300 spectrometer (Germany) with a resonance frequency of 9.77 GHz. The UV–vis absorption spectra were recorded via a UV-2700 spectrophotometer (Shimadzu Corporation, Japan). The high performance liquid chromatography (HPLC) was conducted by Agilent 1260 with a C18 (5 μm, 250 × 4.6 mm) column heated up to 40 °C, and the mobile phase was water/methanol (60/40, v/v) under a flow rate of 0.8 μL/min.

2.4. Catalysis procedures

The catalytic activity of Au NPs/CTS/AC for the hydrogenation of 4-NP was carried out under laboratory condition as described below. In a typical reaction, 5 mg of Au NPs/CTS/AC was added to 50 mL 4-NP (0.2 mM). The mixture solution was stirred for 30 min to reach the adsorption-desorption equilibrium. Then, 0.0757 g of $NaBH_4$ ($C_{4\text{-NP}}/C_{NaBH4}$ = 1/200) was added into the mixture to trigger the reaction with continuous stirring. To monitor the reaction progress, 3 mL of samples was withdrawn at specific intervals time, followed by a filtration with 0.45 μm syringe filter. The absorbance of samples was measured on a UV–vis spectrometer. In order to further confirm the catalytic activity of Au NPs/CTS/AC, the catalytic hydrogenation of 2-NP, 3-NP, 2, 4-DNP, MO, CR and EBT was also conducted under the same conditions. In cycling test, the catalysts were collected via centrifugation, washed by ultrapure water for several times and then dried in vacuum at 50 °C for 24 h for the next cycling reused.

3. Results and discussion

3.1. Characterizations

The comparison of FT-IR spectra provides the information verifying the successful synthesis of CTS/AC composites and the coordination interaction between Au NPs and CTS/AC composites. Fig. 1**A** shows the FT-IR spectra of pristine AC, CTS/AC composites and Au NPs/CTS/AC. In pristine AC spectrum, the peaks at 2362 and 1635 cm^{-1} were ascribed to the C═O vibration and skeletal vibrations from AC [18]. The peaks at 660-880 cm^{-1} were caused by plane bending vibrations of C—H bonds [19]. In the case of CTS/AC, the peaks at 2146 and 1908 cm^{-1} could be assigned to the C—N/N—H groups. The new peaks at 1642 and 1549 cm^{-1} were caused by the amide I (—CONH stretching vibration) and amide II (—NH bending and C—N stretching), which demonstrated the successful synthesis of CTS/AC composites [30]. The decreasing peaks at 800–600 cm^{-1} suggested the interaction between hydrogen or nitrogen of amino groups and oxygen of oxygen-containing groups [35]. As displayed in Fig. 1B, in the spectra of Au NPs/CTS/AC, these peaks shifted slightly due to the complexation of Au NPs and CTS/AC [35]. The crosslinking of functional groups (hydroxyl and amino groups) with Au NPs in the formation of Au NPs/CTS/AC might be responsible for the shifting of the amide band [30]. With Au loading amounts increasing, the peak at 2146 cm^{-1} corresponding to N—H disappeared, indicating that a large number of Au NPs occupied the N—H group of CTS/AC. Meanwhile, the gradual variation in the band region of 800–520 cm^{-1} could be noticed due to Au—N and Au—O bonds stretching vibration [36]. The results illustrated that Au NPs interacted with the hydroxyl and amino groups of CTS/AC.

The morphology and size distribution of synthesized catalysts were recorded by TEM. Fig. 2**A-B** shows a typical low-magnification TEM images of pristine AC and the synthesized CTS/AC. The morphology of pristine AC consists of wrinkles containing some thin layers with porous structure. After decorating with CTS, the AC sheets surface covered with a transparent and relatively smooth thin layers, which implied the CTS coating was formed on the surface of AC. As shown in Fig. 2C, Au NPs anchoring on CTS/AC readily occurred, exhibiting a well dispersion without obvious aggregation on the surface of CTS/AC. Combining the results characterized by FT-IR, it could be concluded that the plenty hydroxyl and amino groups on CTS/AC surface make it an appropriate support for Au NPs anchoring. The existence of Au NPs was further verified by EDS (Fig. S**1**). HRTEM image (Fig. 2D) showed fringes associated with Au lattice appear obviously. The distinct lattice fringes were determined to be 0.235 nm and 0.204 nm, which was corresponded to the Au (111) and Au (220) oriented lattice planes of Au NPs [37]. Fast Fourier Transform (FFT) was calculated for the HRTEM image of Au NPs shown in Fig. 2D, which was consistent with the crystal structure of Au NPs.

XPS was further used to elucidate the surface states of supports (AC and CTS/AC) and catalytically active Au-containing species (Au NPs/$CTS/AC_{(4)}$). Fig. 3 displayed the core energy level XPS spectra of C 1s, N 1s, O 1s and Au 4f. In C 1s spectra of all samples, the five specific signals were corresponded to C—C (284.6 eV), C—OH (285.1 eV), C—N (286.6 eV), N—C═O (287.7 eV) and C—O (288.8 eV), respectively. Compared C 1s spectra of CTS/AC with AC, the peaks intensity of C—N and N—C═O increased. It might because the CTS, with a high C/O ratio and each nitrogen atom corresponding to at least six carbon atoms and four oxygen atoms [30], has been absorbed onto AC. And the peak intensity of C—OH decreased, which might be related to the occupation of CTS on the oxygen-containing groups of AC surface [30]. In the C 1s spectra of Au NPs/$CTS/AC_{(4)}$, the peak intensity of C—OH and N—C═O decreased. In N 1s spectra of CTS/AC, the peaks at 400.0 and 401.8 eV were attributed to $N-(C)_3$ and N—H, which also evidenced that the CTS/AC composites were successfully synthesized. After Au NPs loading, the peaks in N 1s spectra of Au NPs/CTS/AC shifted to a higher binding energy (400.4 and 402.2 eV), indicating the interaction between Au NPs and CTS/AC supports. Furthermore, it can be concluded that the nitrogen terminals in the N—H serve as the anchor for Au NPs on CTS/AC [38,39]. In addition, compared O 1s spectra of Au NPs/CTS/AC with CTS/AC composites, the peak at 531.7 eV shifting to a higher binding energy 532.2 eV has also been observed, further verifying an interaction between Au NPs and supports. In the high-resolution spectra of Au 4f, the peaks at 84.2 and 87.9 eV were ascribed to Au $4f_{7/2}$ and Au $4f_{5/2}$ of metallic Au^0 (the peak-to-peak distance is 3.7 eV). The formed Au^0 is owing to the high reducibility of hydroxyl and amino groups on CTS/AC surface [40]. In addition, the distinct additional peaks on the high binding energy side could be assigned to the oxidation states of Au^+ (green devolution) and Au^{3+} (orange devolution) [41,42], indicating the partial reduction of $HAuCl_4$ during synthetic process. It has been reported that the oxidation states of Au (Au^+ and Au^{3+}) could be formed and stabilized on the hydroxyl groups on the supports surface via forming Au—O interfacial bonds [42] and played a positive role in

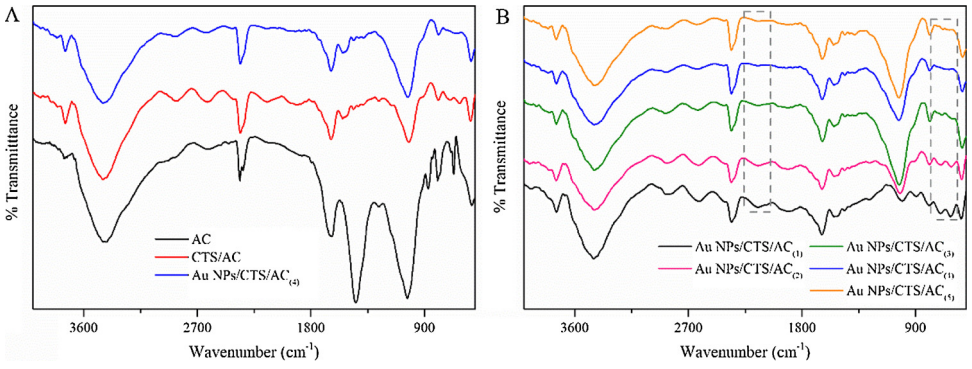

Fig. 1. FT-IR spectra of (A) pristine AC, CTS/AC and Au NPs/CTS/AC, (B) Au NPs/CTS/AC with different Au loading amounts.

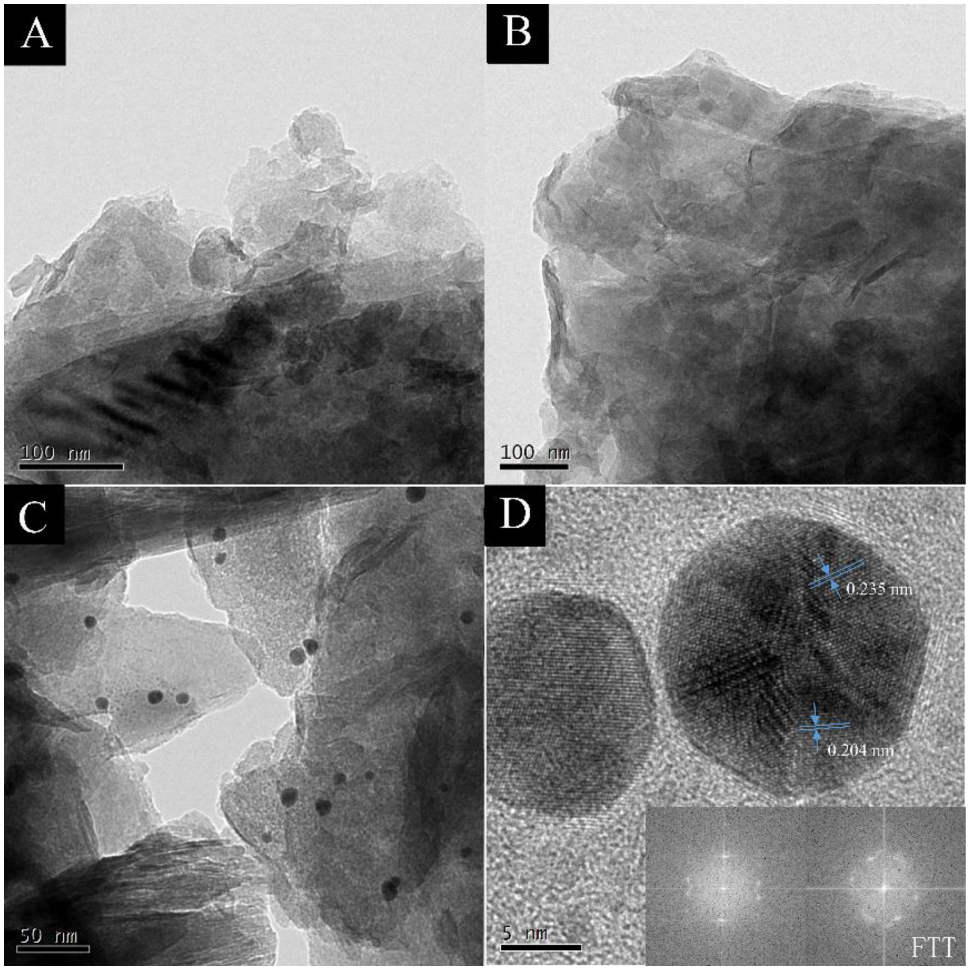

Fig. 2. TEM images of (A) pristine AC, (B) CTS/AC composites, (C) Au NPs/CTS/AC and (D) HRTEM images of Au NPs/CTS/AC. The insets are FTT images corresponding to the Au NPs crystals.

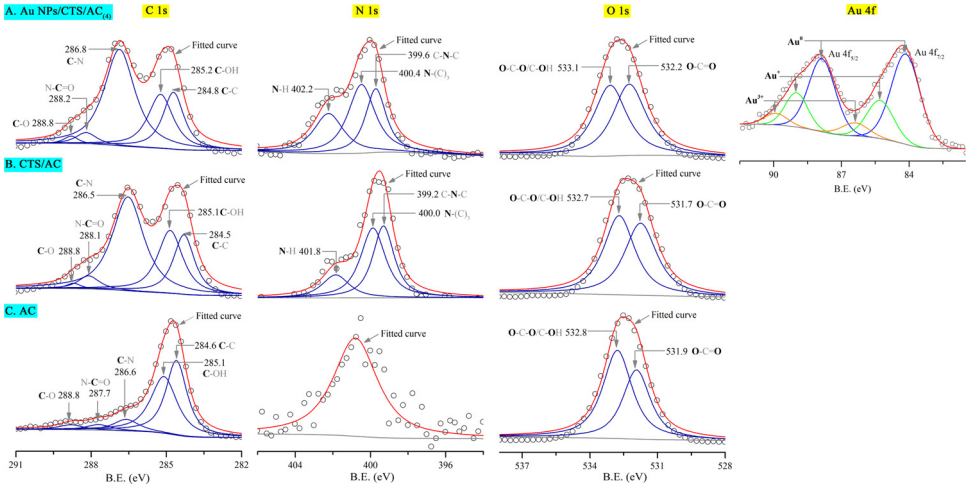

Fig. 3. Comparative core energy level XPS of (A) Au NPs/CTS/$AC_{(4)}$, (B) CTS/AC and (C) AC.

the hydrogenation of 4-NP [40].

Further XRD studies were conducted to compare the crystalline nature of AC, CTS/AC and Au NPs/CTS/AC. As shown in Fig. 4, the XRD pattern of pristine AC showed a strong intense diffraction peak centered at 26.62°, which could be ascribed to hexagonal lattice of a graphite-like layer crystallite structure [17]. The minor peaks centered at 20.9°, 50.1° and 68.1° were attributed to the trace quantity of inert element silica [43], which was identified by the EDS spectra of AC (Fig. S1**A**). In the XRD pattern of Au NPs/CTS/AC, the peaks at 2θ = 38.2°, 44.4°, 64.6° and 77.8° were attributed to face-centered cubic (fcc) Au of (111), (200), (220) and (311), respectively, corresponding to the standard values in XRD card of Au (JCPDS No.04-0784).

The H_2-TPR was conducted to explore the reduction behavior of the supported Au NPs catalysts. For pristine AC, as shown in Fig. 5A, the

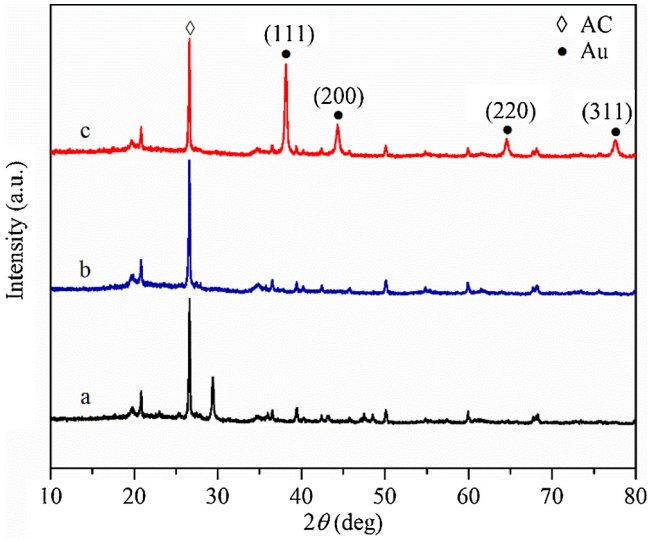

Fig. 4. X-ray diffraction spectra of (a) pristine AC, (b) CTS/AC and (c) Au NPs/CTS/$AC_{(4)}$.

appearance of TCD signal was observed in the temperatures of 300–780 °C. To further analyze the results, the mass spectrometry detection was conducted to record the gas products (NO, CO_2 and H_2O) during TPR test. The mass spectra (Fig. S**2** and Table S**1**) showed that NO, CO_2 and H_2O were generated in the temperatures of 500–600 °C. The formation of NO and CO_2 could be ascribed to the decomposition of a part of AC from the leaching of N, O and the decomposition of a part of AC network. It is in well agreement with the result reported by Truszkiewicz et al [44]. It is known that before the TPR test, the sample would be purge treated under a pure He flow for 2 h, which was aimed at the removal of moisture in sample. Hence, the formation of H_2O in the temperatures of 500–600 °C, which might because the H_2 reacted with surface oxygen species or lattice oxygen [17]. Therefore, the TCD signal in the temperatures of 500–600 °C could be ascribed to the decomposition of a part of AC from the leaching N, O and the decomposition of a part of AC network as well as the reduction of surface oxygen species or lattice oxygen. In addition, NO was formed in the temperatures of 700–780 °C, which could also be ascribed to the decomposition of a part of AC from the leaching of N, O and the decomposition of a part of AC network.

For Au NPs/CTS/AC with different Au loading amount, as shown in Fig. 5B, the TCD signal in the temperatures of 350–450 °C was ascribed to the reduction of Au^{3+} to Au^0, corresponding to the previous results elicited by XPS analysis. It can further illustrate the interaction between Au NPs and CTS/AC, and the presence of oxidation state Au species on CTS/AC supports. Besides, it is interesting to note that the TCD signal around 500 °C appeared when Au loading amount increased, while the TCD signal was absent in a relatively low Au loading amount. It could be attributed to the reduction of surface oxygen groups during the formation of Au—O on the CTS/AC surface [45]. In addition, when the Au loading amount increased, the TCD signal in the temperatures of 500–600 °C shifted to lower temperature. It could be ascribed to the hydrogen spillover, i.e. the atomic H migrated to the neighboring supports after H_2 dissociation on the Au surface. Subsequently, it promoted the reduction of surface oxygen species on the supports at lower temperature, resulting in the peak shifting to lower temperature [45]. As reported by Li et al., the lower reduction temperature of catalysts is, the higher reducibility the catalysts possess, causing the good catalytic activity [17]. Therefore, Au NPs/CTS/AC is endowed with reducibility with the aid of Au NPs and thus generates more active surface species, which is conducive to form the Au—H intermediates in the 4-NP hydrogenation and important for enhancing catalytic performance [17].

3.2. Catalytic performance of Au NPs/CTS/AC catalyst for nitrophenols hydrogenation

3.2.1. Catalytic activity for 4-NP hydrogenation as a model reaction

The catalytic activity of the as-prepared Au NPs/CTS/AC catalysts was evaluated through the catalytic hydrogenation of 4-NP as a model reaction. Pristine AC and CTS/AC were also used for comparison. As shown in Fig. S**3A**, after adding $NaBH_4$ to the 4-NP with a color changing from light yellow to yellow green, 4-nitrophenolate ions were formed which showed a strong absorbance at 400 nm. The hydrogenation of 4-NP was negligible in the presence of $NaBH_4$ without any catalyst, indicating no hydrogenation occurred for 4-NP during reaction time of 1 h because of the kinetic barrier. Only about 14% adsorption occurred in the presence of AC, while almost 7% adsorption occurred with CTS/AC under the same experimental conditions. Compared to the blank experiments, as-prepared Au NPs/CTS/AC catalyst exhibited substantially enhanced catalytic performance. Fig. 6**A** shows typical UV–vis absorption spectra at different time interval after adding of Au NPs supported on CTS/AC. It is obvious that the absorbance peak at 400 nm decreased as the reaction proceeds, because of the hydrogenation of 4-NP. Simultaneously, a new peak appeared at 300 nm on account of the formation of 4-AP [10]. In order to confirm the product, the determination of 4-AP was recorded with UV–vis absorption spectra (Fig. S**3B**), demonstrating there was no byproduct during hydrogenation of 4-NP. Considering $NaBH_4$ was in excess ($C_{4\text{-NP}}/C_{NaBH4}$ = 1/200), this reaction kinetics could be assumed as pseudo-first-order kinetics with a rate constant k_{app} of 0.6994 min^{-1} (Fig. 6B). In addition, the catalytic hydrogenation was analyzed by the HPLC technique. Fig. S**4** showed the retention time of standard 4-NP solution (0.2 mM) and 4-AP (0.2 mM) were standardized as 7.03 min and 5.22 min, respectively. And the peak ascribed to 4-NP disappeared and the peak ascribed to 4-AP appeared at the final stage of reaction. Hence, the conversion of 4-

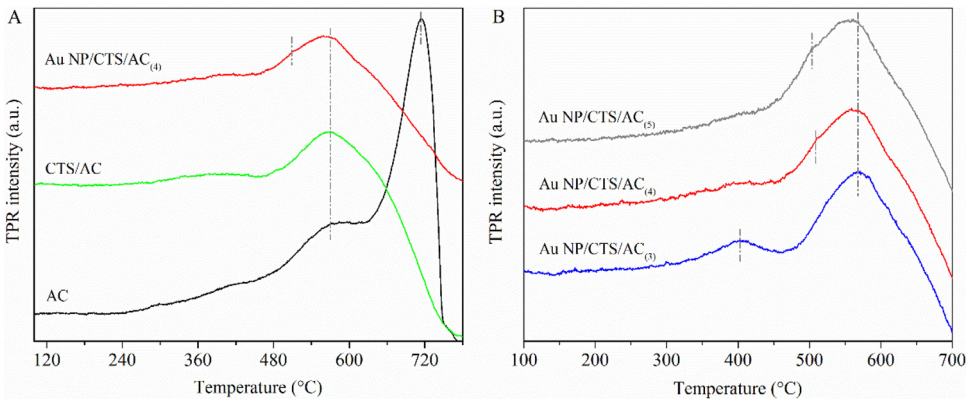

Fig. 5. H_2-TPR profiles of (A) pristine AC, CTS/AC and Au NPs/CTS/AC, (B) Au NPs/CTS/AC with different Au loading amounts.

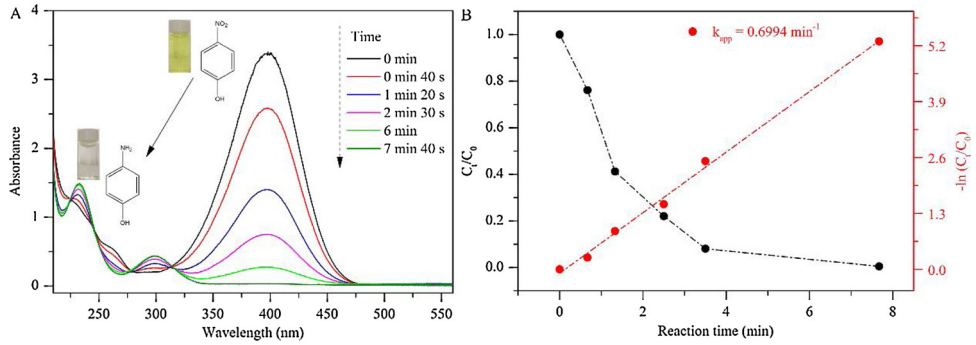

Fig. 6. (A) Time-dependent UV–vis absorption spectra and (B) plots of C_t/C_0 and -ln (C_t/C_0) versus time of the hydrogenation of 4-NP catalyzed by Au NPs/CTS/$AC_{(4)}$.

NP was determined as 100%. Based on the standard curve from HPLC chromatograms, the yield of 4-AP was determined as 98%.

3.2.2. Effect of different Au loading amounts

In order to optimize Au NPs/CTS/AC catalysts, we have investigated the effect of Au loading amounts on the catalytic activity. The catalytic activity in terms of 4-NP hydrogenation over Au NPs/CTS/AC catalysts with different Au loading amount is shown in Fig. 7 and **Table S2**. With the increase of Au loading amount from 0.0014 wt% to 2.5033 wt%, the catalytic activity initially increased and then decreased. As shown in **Fig. S5A-D**, it can be inferred that the initial enhancement of catalytic activity could be ascribed to the increased effectively active sites. Then, as the loading amount increased to 2.5033 wt%, the Au NPs were aggregated into large size distribution owing to the excessive Au loading amount, thereby resulting in a decrease of catalytic activity (**Fig. S5E**). In addition, the excessive Au loading amount (2.5033 wt%) would lead to the jam-up inside the chitosan matrix on the surface of AC, i.e., the mass transfer of 4-NP into the catalytic sites of CTS/AC would be hampered, resulting in the decrease of catalytic activity. In the case of the Au NPs/CTS/$AC_{(4)}$, the appropriate Au loading amount lead to relatively small size distribution, which could provide more effectively active sites for 4-NP hydrogenation. Hence, the Au NPs/CTS/$AC_{(4)}$ showed the higher catalytic activity. In addition, based on the analyses reported by Ye et al [45], the dispersion of Au NPs in Au NPs/CTS/$AC_{(4)}$ was calculated to be 9.09% according to TEM images. Compared with the previous reported Au-based catalysts, the dispersion of Au in our study was satisfactory [37,45].

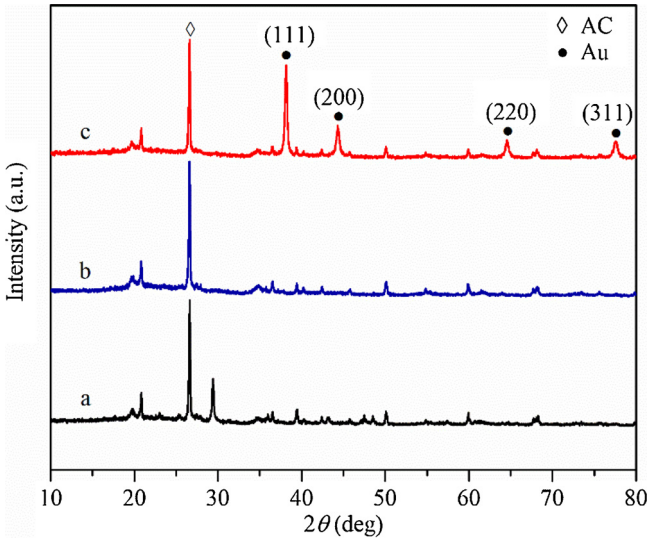

Fig. 7. (A) C_t/C_0 and (B) -ln (C_t/C_0) versus reaction time for the hydrogenation of 4-NP over Au NPs/CTS/AC with varying loading Au amounts, respectively.

Meanwhile, turnover frequency (TOF) was calculated for the reaction with the optimum catalyst Au NPs/CTS/$AC_{(4)}$. The TOF of the catalyst in our study is 202 h^{-1}, which is comparable or even superior to the catalysts recently reported. Besides, to properly investigate catalytic activity and compare with other catalysts recently reported, **Table S3** lists the reaction time, the rate constant and the normalized rate constant with regard to the catalysts dosage and Au loading amounts as well as the TOF of the optimum catalyst Au NPs/CTS/$AC_{(4)}$. It can be seen that our catalyst Au NPs/CTS/$AC_{(4)}$ exhibits comparable or even superior catalytic performance and TOF when compared with other catalysts previously reported.

3.2.3. Effect of environmental water samples

To better simulate the catalytic hydrogenation of 4-NP in real wastewater, the effect of environmental water samples has been taken into discussion. Thus, we used various environmental water samples such as tap water, lake water and river water (**Fig. S6 and S7**) as solvent to dissolve 4-NP as reaction solution to study the catalytic hydrogenation of 4-NP using Au NPs/CTS/$AC_{(4)}$ and check whether the prepared catalyst could maintain the high catalytic activity in real water samples. Fig. 8**A** displayed that the catalytic hydrogenation of 4-NP could be conducted over Au NPs/CTS/$AC_{(4)}$ under various environmental water and the rate constant k_{app} was 0.6994, 0.5728, 0.2707 and 0.1753 s^{-1} corresponding to ultrapure water, tap water, lake water and river water, respectively.

Nonetheless, the various hydrogenation rates catalyzed by Au NPs/CTS/$AC_{(4)}$ indicated that the catalytic performance was inhibited in some extent and the hydrogenation rate of 4-NP in river water was the lowest. The various catalytic rate may be the result of the different water condition such as pH value, DO and co-existent ions [46]. Although the mixture solution would be alkaline after the final addition of $NaBH_4$, the amount of 4-NP adsorbed onto the surface of Au NPs/CTS/$AC_{(4)}$ catalysts was different before the addition of $NaBH_4$, thereby affecting the catalytic rate. Hence, the initial pH would affect the catalytic activity to some extent. In detail, the influence of initial pH on the catalytic activity was mainly related to the pH_{IEP} of catalysts and pK_a of reactant [46]. The measured pH_{IEP} of Au NPs/CTS/$AC_{(4)}$ was at about pH 7 (**Fig. S8**), indicating the catalysts were negatively charged at pH < 7. The pK_a value of 4-NP is 7.2, indicating that the 4-NP tend to deprotonate to nitrophenolate ions in the anionic form at pH < 7.2. Hence, in the lake water (pH value of 7.54) and river water (pH value of 7.79), the surface of Au NPs/CTS/$AC_{(4)}$ and the nitrophenolate ions were negatively charged and led to the electrostatic repulsion, thereby decreasing the catalytic activity. The Zeta potential of catalysts in tap water (pH value of 7.05) was close to the isoelectric point, which had less effect on the adsorption of 4-NP onto the Au NPs/CTS/$AC_{(4)}$ catalysts surface. In addition, previous studies have reported that dissolved oxygen (DO) would outcompete 4-NP for reductant $NaBH_4$, i.e., oxygen dissolved in water would consume some $NaBH_4$, leading to a decrease of catalytic activity [37,47]. Besides, the DO of lake water and river

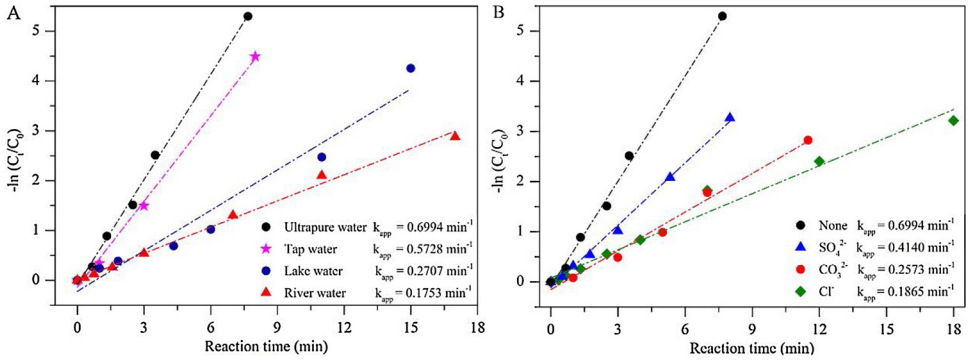

Fig. 8. (A) Catalytic hydrogenation of 4-NP in ultrapure water, tap water, lake water and river water; (B) Effect of inorganic salt (SO_4^{2-}, Cl- and CO_3^{2-}) on the hydrogenation of 4-NP by Au NPs/CTS/$AC_{(4)}$. [4-NP] = 0.2 mM; [$NaBH_4$] = 0.04 M; [All inorganic salt] = 0.5 mM; m (Au NPs/CTS/$AC_{(4)}$) = 5 mg.

water was measured to be 3.06 and 6.12 mg/L, indicating there was less competition for $NaBH_4$ between DO and 4-NP in lake water, and thus more $NaBH_4$ was available for hydrogenation of 4-NP. This can explain that the catalytic hydrogenation activity of Au NPs/CTS/$AC_{(4)}$ in lake water was better than that in river water. Thereby, the effects of DO and pH made the catalytic activity decrease in lake water and river water. Moreover, the existence of other competitive pollutants and common ions in lake water and river water would result in the lower catalytic activity [5]. Nevertheless, in relatively short time, the eventual removal efficiency could reach 100% under different water samples (**Fig. S7**), demonstrating that the prepared catalyst has the potential for the hydrogenation of nitrophenols in wastewater treatment in environmental water samples.

3.2.4. Effect of inorganic salt

Inorganic salt is common and coexists with organic pollutant in real environmental water, which is different from ultrapure water, and may influence the catalytic activity of catalysts. As shown in Table 1, SO_4^{2-} and Cl- with different content exist in different environmental water samples. Thus, it is necessary to investigate their effects on the hydrogenation of 4-NP, to further explain the results of various hydrogenation rate of 4-NP under different water samples. Herein, Na_2SO_4, NaCl and Na_2CO_3 were added to explore the detail effects on the catalytic hydrogenation of 4-NP.

Fig. 8**B** displays the results of 4-NP hydrogenation in the presence of above common anions at a concentration of 0.5 mM. The catalytic efficiency of 4-NP with these anions could reach 100% within 18 min (**Fig. S9**) and the corresponding order of the hindering effect of these anions was as follows: $Cl^- < CO_3^{2-} < SO_4^{2-}$. A slight negative effect could be found in the presence of SO_4^{2-} with the rate constant of 0.4140 min^{-1}. It was consistent with the result that in spite of higher SO_4^{2-} content in river water (Table 1), it had no influence on the catalytic activity of Au NPs/CTS/$AC_{(4)}$. The obvious negative effects were found in the presence of CO_3^{2-} and Cl^-. It could be speculated that CO_3^{2-} was prone to combine with hydrogen ions to produce HCO_3^{2-} and OH^- after ionization in water, thus making the pH value of water weakly alkaline and a decrease of catalytic activity. It was in accordance with the above result of catalytic hydrogenation in the river water with relatively high pH. Besides, the existence of HCO_3^- and OH^- can accelerate the hydrolysis rate of $NaBH_4$ thereby resulting in hydrogen release [48], which can be ascribed to the attack of negative hydrogen ions in $NaBH_4$ by positive hydrogen ions in the HCO_3^- and OH^-. The excessive hydrogen production would result in the release of H_2 from reaction solution and consumption of a large number of hydrogen resource, thereby inhibiting the catalytic rate in some degree. Especially, the existence of Cl^- retarded the reaction rate, which was different from the result reported by Doong et al [46]. It could be ascribed to the catalyst poisoning caused by Cl^- [37]. Besides, the competitive adsorption between Cl^- and 4-NP on the surface of the catalyst could lead to the negative effect of 4-NP hydrogenation [46], which explained the lower catalytic activity in river water with higher content of Cl^-. In addition, the Zeta potentials of the reaction solution in the presence of Au NPs/CTS/$AC_{(4)}$ and above anions were tested to illustrate difference between various reaction condition and listed in Table 2, with the following order: $SO_4^{2-} < CO_3^{2-} < Cl^-$. The Zeta potential (−10.19 ± 1.47 mV) in the presence of SO_4^{2-} were closer to that (−10.04 ± 1.31 mV) of the reaction condition without any anions. In contrast, the Zeta potential (−0.11 ± 0.04 mV) in the presence of Cl^- decreased, further to testify the negative effect with the lower Zeta potentials.

Table 1
The dissolved oxygen (DO), pH value and common anions content in different water matrix.

Water matrix	Ultrapure water	Tap water	Lake water	River water
DO (mg/L)	7.29	6.48	3.06	6.12
pH value	6. 73	7.05	7.54	7.79
SO_4^{2-} (mg/L)	–	17.2	14.7	22.5
Cl^- (mg/L)	–	0.058	0.074	0.084

3.2.5. Catalytic activity of various nitrophenols

To further study the scope and generality of as-prepared Au NPs/CTS/$AC_{(4)}$ catalyst, catalytic hydrogenation of other nitrophenols with different substituent (2-NP, 3-NP and 2, 4-DNP) were also conducted under the same conditions. **Fig. S10** showed that all the nitrophenols could be degraded efficiently catalyzed by Au NPs/CTS/$AC_{(4)}$ in a relatively short time. The strongest a absorbance bands at 283 nm (2-NP), 333 nm (3-NP) and 448 nm (2, 4-DNP) in the presence of $NaBH_4$ and their absorbance bands gradually decreased as the hydrogenation proceeds upon the addition of Au NPs/CTS/$AC_{(4)}$. The color of all reactant mixture varied from their natural color to colorless (**Fig. S11**), indicating the hydrogenation finished completely. The catalytic efficiency was different with the rate constant k_{app} in the order by 4-NP (0.6994 min^{-1}) > 3-NP (0.3989 min^{-1}) > 2-NP (0.3781 min^{-1}) > 2, 4-DNP (0.2654 min^{-1}). It could be ascribed to the molecular orientation of nitro-substituent [46]. The negatively charged O atoms on 4-NP ions can be delocalized throughout the benzene ring and become more resonance-stabilized than those of 2-NP and 3-NP [49,50]. In addition, the number of nitro-substituent also have an impact on determining the reactivity of nitrophenols [37]. Hence, 4-NP showed a better reactivity than that of 2-NP, 3-NP and 2, 4-DNP.

3.2.6. Recycling stability of catalyst

The recycling stability of catalysts is a key issue in practical applications. The Au NPs/CTS/$AC_{(4)}$ was reused six times in the same process to estimate its catalytic stability. As displayed in Fig. 9A, the catalytic activity of Au NPs/CTS/$AC_{(4)}$ has no apparent deactivation even

Table 2
Zeta potentials of the reaction solution in the presence of Au NPs/CTS/$AC_{(4)}$ and different common anions.

Common anions	None	Na_2SO_4	NaCl	Na_2CO_3
Zeta potential (mV)	−10.04 ± 1.31	−10.19 ± 1.47	−0.11 ± 0.04	−6.97 ± 0.78

Experimental conditions: [4-NP] = 0.2 mM; [$NaBH_4$] = 0.04 M; [All inorganic salt] = 0.5 mM; m (Au NPs/CTS/$AC_{(4)}$) = 5 mg.

after six successive recycles for the hydrogenation of 4-NP, with the conversion of 4-NP dropping from 100% to 90% within reaction time of 7 min 40 s. The XRD spectra in Fig. 9**B** shows that the diffraction peaks corresponding to metallic Au^0 enhanced slightly, which could be ascribed to the reduction of a small amount of Au^+ and Au^{3+} species to metallic Au^0 in the presence of the reductant $NaBH_4$. Besides, the XPS results (Fig. 9**C-D**) displayed that although a small part of Au^+ and Au^{3+} species were reduced to metallic Au^0 after catalytic reaction, a number of Au^+ and Au^{3+} species exist in the used catalysts. It might because the Au^+ and Au^{3+} species stabilized on the hydroxyl groups made that the reduction of Au^+ and Au^{3+} species into Au^0 was difficult in comparison of the reduction of isolated Au^+ and Au^{3+} species [42]. In addition, $NaBH_4$ preferentially participated in the catalytic hydrogenation of 4-NP, resulting in that few $NaBH_4$ participated in the reduction of Au^+ and Au^{3+} species. Hence, the used catalysts had no obvious change in the chemical states after catalytic reaction, indicating the stability of catalysts. In comparison to Au NPs catalysts recently reported and previous research in our group, the stability of Au NPs/CTS/AC is improved noticeably [37]. Therefore, the presence of CTS could effectively improve the stability of Au NPs on account of positive electricity and abundant reactive hydroxyl and amino functional groups of CTS.

3.3. Mechanism of synthesis of Au NPs/CTS/AC and 4-NP hydrogenation

Based on the aforementioned results, the mechanism of the synthesis of Au NPs/CTS/AC and 4-NP hydrogenation catalyzed by Au NPs/CTS/AC catalysts was proposed (Scheme 1). It can be seen that the reaction conditions of preparation and catalytic hydrogenation is green owing to 100% toxicity chemical-free, the utilization of natural polymer with biocompatibility and reaction under mild condition (room temperature).

3.3.1. Synthesis of Au NPs/CTS/AC

The CTS/AC composites were successfully synthesized, which could be ascribed to the surface charge and functional groups of CTS and AC surface. The Zeta potential of CTS and AC in solution was measured to be +52.5 mV and -2.51 mV, respectively, indicating the electrostatic interaction between CTS and AC. Besides, the hydrogen or nitrogen of amino groups on CTS would bond with oxygen of oxygen-containing groups on AC, making interaction between CTS and AC [35]. It was supported by the FT-IR results. Hence, the functional groups on CTS and AC surface could also be the driving force for the synthesis process. In addition, the entangled polymer chains of CTS was beneficial for the interaction between CTS and AC [36]. After the addition of $HAuCl_4$, plenty hydroxyl and amino groups on surface of CTS were exposed to Au (III), thus leading to the formation of Au NPs. It can be validated by the phenomenon that the surface concentration of N—H species

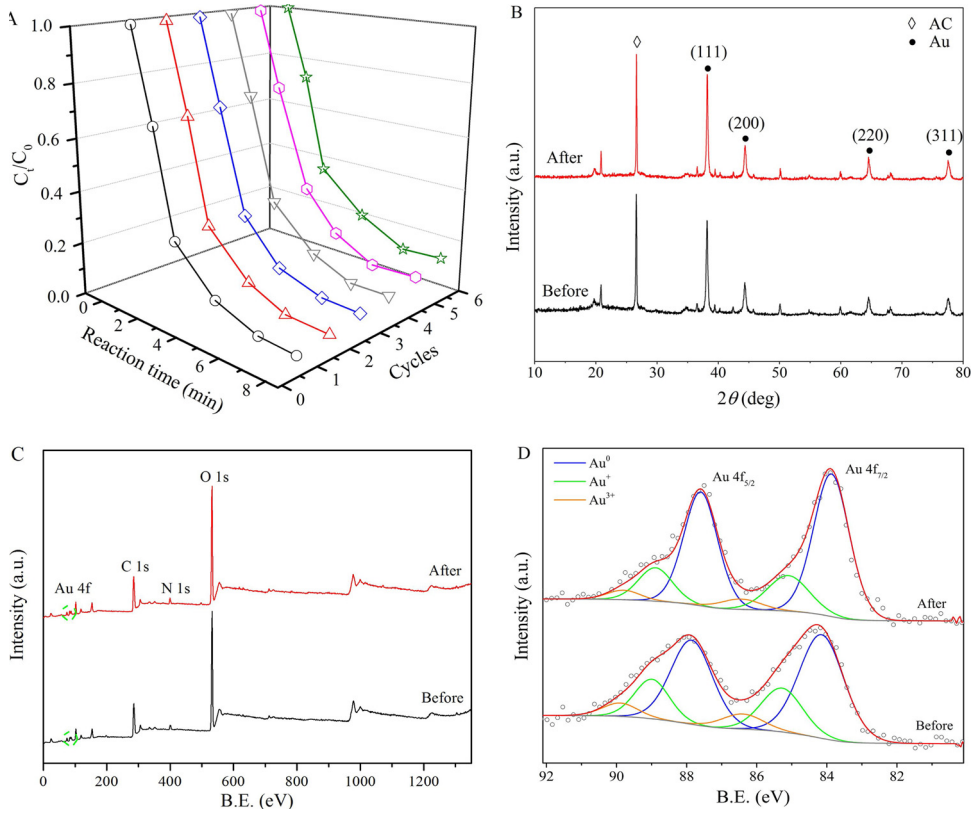

Fig. 9. (A) Recycling test for the catalytic hydrogenation of 4-NP (0.2 mM, 50 mL) by Au NPs/CTS/$AC_{(4)}$ (5 mg). (B) XRD spectra, (C) XPS survey and (D) high-resolution spectra of Au 4f of catalysts before and after catalytic hydrogenation.

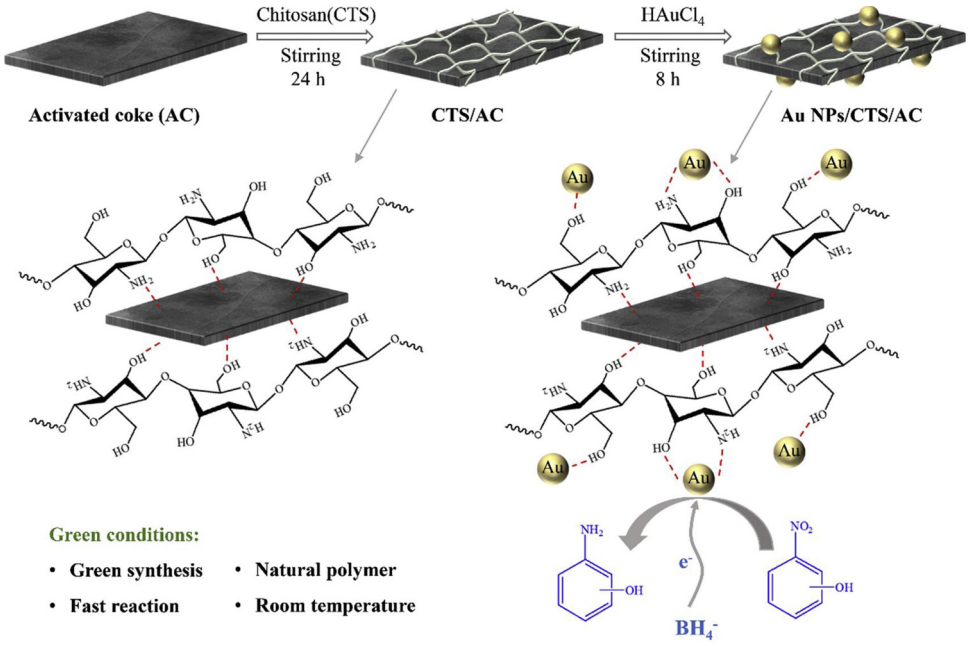

Scheme 1. The mechanism of preparation of Au NPs/CTS/AC catalysts and catalytic hydrogenation of nitrophenols.

decreased with Au^0 formation in XPS spectra, providing evidence that Au NPs might be trapped by nitrogen terminals of N—H species in the composites [38]. This is consistent with the observation from the FT-IR spectra of Au NPs/CTS/AC. It has been reported that the growth process of metal NPs is related to the nature of the support [38]. Thus, the CTS/AC surface chemistry played an important role in the determining Au NPs size and dispersion. (i) The hydroxyl and amino groups on CTS/AC would prevent the aggregation of Au NPs, guaranteeing the dispersion of Au NPs on CTS/AC surface. (ii) The surface of CTS/AC was positively charged owing to the plenty amino groups of CTS, while Au NPs are generally negatively charged without capping agents. Thus, CTS/AC could immobilize Au NPs through complexing or electrostatic interaction, preventing the aggregation of Au NPs [29]. (iii) In the synthetic process, the high agitation speed of 900 rpm was beneficial to the formation of Au NPs dispersedly anchoring on CTS/AC surface.

3.3.2. Au NPs/CTS/AC catalytic hydrogenation of nitrophenols

To figure out the specific role of Au NPs in the catalytic system, EPR with DMPO as the spin trapper was used to explore the mechanism of 4-NP hydrogenation over Au NPs/CTS/$AC_{(4)}$. As shown in Fig. 10A, no obvious EPR signal was detected in the absence of Au NPs/CTS/$AC_{(4)}$ or $NaBH_4$, but the signal that consisted of a 1:1:1 triplet of 1:2:1 triplet was detected in the presence of $NaBH_4$, which was identified as a DMPO-H adduct by comparison with previous studies [46]. It indicates that the BH_4^- would generate the H· radical adducts via dissociation of the B—H bond. Nonetheless, the intensity of DMPO-H signal enhanced in the presence of Au NPs/CTS/$AC_{(4)}$ + $NaBH_4$, illustrating the DMPO-H adducts most likely came from the abstraction of hydrogen of the active sites Au NPs [46]. Based on the Langmuir-Hinshelwood model reported by Ballauff et al., BH_4^- reacts with Au NPs to form Au—H intermediates via the dissociation of B—H bond [51]. Thus, the presence of Au NPs would assist the dissociation of B–H bonds and hence promote the abstraction of hydrogen from $NaBH_4$ to form Au-H intermediates. Then, the H· radical adducts of Au-H intermediates would attack the positively charged nitrogen in the nitro group of 4-NP, catalyzing the hydrogenation of nitrophenols to the corresponding amine (Fig. 10B). After H· radical attack to the nitro group, the Au^+ species could be regenerated, continuously forming a new Au—H intermediates to complete the catalytic hydrogenation [52].

The Au NPs/CTS/$AC_{(4)}$ exhibits enhanced catalytic activity for nitrophenols hydrogenation. Combining the EPR results and XPS analysis of Au NPs/CTS/$AC_{(4)}$, it can be inferred that one of the reasons is the presence of oxidation state of Au (Au^+ and Au^{3+}), which would accelerate the electron transfer from a hydride (H^-) source (BH_4^-) to nitrophenols in the hydrogenation process, in which corresponding amine is the product of the six electron reduction of 4-NP [14]. And the

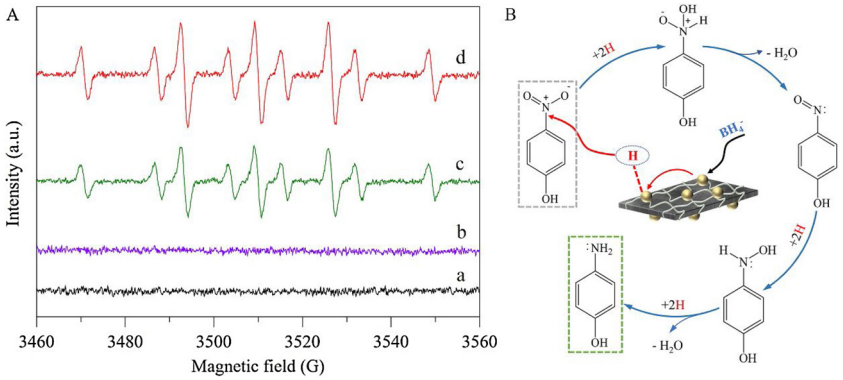

Fig. 10. (A) EPR spectra of DMPO-H adducts formed in the presence of (a) 4-NP + CTS/AC, (b) 4-NP + Au NPs/CTS/$AC_{(4)}$, (c) 4-NP + $NaBH_4$, and (d) 4-NP + $NaBH_4$ + Au NPs/CTS/$AC_{(4)}$. (B) Proposed reaction pathway for the 4-NP hydrogenation by $NaBH_4$ over Au NPs/CTS/$AC_{(4)}$.

existence of Au^{+} and Au^{3+} could readily form reactive Au−H intermediates via dissociation of the B−H bond [52]. Thus, the Au^{+} and Au^{3+} could serve as an electron relay system and hydride transfer agents [40], enhancing the catalytic activity of the Au NPs/CTS/$AC_{(4)}$. Besides, it is well-known that the well-dispersion of Au NPs would guarantee the catalytic activity. Hence, another reason is related to the plenty hydroxyl and amino groups on CTS/AC surface, which can promote an improved dispersion of the Au NPs in appropriate loading amount and thus provide more effective active sites.

3.4. Catalytic performance of Au NPs/CTS/AC catalyst for azo dyes hydrogenation

3.4.1. Catalytic activity for azo dyes (MO, CR and EBT) hydrogenation

The wastewater containing azo dyes would cause serious problem to water environment and human health. It is well reported that the cleavage of azo bond (−N═N−) in hydrogenation would eliminate toxic substances and could effectively done by various metal NPs [16,53]. Hence, several azo dyes (MO, CR and EBT) were also taken as pollutants to investigate the catalytic activity of Au NPs/CTS/$AC_{(4)}$ catalysts. Firstly, the Au NPs/CTS/AC catalysts were used to absorb the dyes. As shown in **Fig. S12**, the characteristic peaks of MO, CR and EBT decreased slightly within 30 min and the color remained unchanged. After the additional of $NaBH_4$ serving as hydride source, the corresponding peaks of MO (465 nm), CR (496 nm) and EBT (615 nm) decreased rapidly (**Fig. S13A-C**) with the decolorization of solutions (**Fig. S11**). Simultaneously, the new peak at around 250 nm appeared, indicating the new colorless compounds were formed. The new peak of the colorless compounds might be attributed to the two sides of the cleavage azo bonds or their derivatives [54]. As shown in **Fig. S13D,** the rate constants were calculated to be 1.0244, 1.3722 and 0.5642 min^{-1} for MO, CR and EBT, respectively. The degradation rate of MO and CR was much faster than that of EBT, which can be ascribed to their different adsorption abilities of Au NPs/CTS/AC towards these azo dyes and different structure formulas of azo dyes [32,55]. Nevertheless, the Au NPs/CTS/AC catalysts exhibited remarkable catalytic activity towards various azo dyes.

3.4.2. Catalytic hydrogenation pathway for azo dyes

To further confirm the degradation process of azo dyes (MO, CR and EBT) and composition of colorless compounds, the degradation products were analyzed by liquid chromatography-mass spectrometry (LC−MS). For the hydrogenation of MO, the main signals at *m/z* 172.12 and 137.02 could be found in LC−MS spectra (**Fig. S14A**). The *m/z* 172.12 and 137.02 were attributed to the molecular formula of $C_6H_6NO_3S^-$ and $C_8H_{12}N_2$ (**Fig. S14B**), respectively. It indicates that the −N═ bond on the original MO molecule was split by catalytic hydrogenation, resulting in the decolorization of solutions. For the hydrogenation of CR, the main signals at *m/z* 326, 221.16 and 184.03 were observed in LC−MS spectra (**Fig. S15A**), which were corresponded to different probable intermediates such as $C_{16}H_{12}N_3O_3S^-$, $C_{10}H_8NO_3S^-$ and $C_{12}H_{12}N_2$ [56]. As shown in **Fig. S15B**, the −N═N− bonds of CR molecular were gradually split to aromatic intermediates with small molecular weight by catalytic hydrogenation. Similar to the hydrogenation of MO and CR, the hydrogenation pathway of EBT was depicted in **Fig. S16**. These results indicates that the decolorization of azo dyes was related to the hydrogenation of −N═N− to −NH−NH− and then the cleavage of −NH−NH bonds [32,54].

4. Conclusions

In summary, the Au NPs/CTS/AC catalysts were prepared via a green synthesis, in which CTS not only acted as a mild reductant and a linker between AC and Au NPs, but also stabilized Au NPs, preventing their aggregation. The size distribution and morphology of Au NPs on CTS/AC could be conveniently controlled by adjusting the addition dosage of $HAuCl_4$. For the model catalytic hydrogenation of 4-NP by $NaBH_4$, the Au NPs/CTS/AC catalysts exhibited much better catalytic performances than other Au NPs catalysts recently reported in terms of the catalytic activity (reaction completed within 7 min 40 s), reaction rate constant (0.6994 min^{-1}) and TOF (202 h^{-1}). In addition, the catalysts exhibited high catalytic activity in various environmental water samples and in the presence of various inorganic salt, indicating the satisfying application potential. The catalysts also exhibited well generality in the reduction of various substituted nitrophenols (2-NP, 3-NP, 4-NP and 2, 4-DNP) and azo dyes (MO, CR and EBT), and showed good recyclability with the catalytic performance remained 90% within 7 min 40 s over six recycles. This work provides a green pathway for the synthesis of Au NPs-based catalysts and the as-prepared catalysts exhibit a great potential in real-world environmental purification applications for nitrophenols hydrogenation.

Acknowledgements

The authors would like to thank Ning Yan for his assistance with the TEM measurements. This study was financially supported by the Program for the National Natural Science Foundation of China (51879101, 51579098, 51779090, 51709101, 51521006, 51809090, 51278176, 51378190), the National Program for Support of Top–Notch Young Professionals of China (2014), the Program for Changjiang Scholars and Innovative Research Team in University (IRT-13R17), and Hunan Provincial Science and Technology Plan Project (2018SK20410, 2017SK2243, 2016RS3026), and the Fundamental Research Funds for the Central Universities (531119200086, 531118010114, 531107050978). Hunan Provincial Innovation Foundation for Postgraduate (CX2018B155).

Appendix A. Supplementary data

Supplementary material related to this article can be found, in the online version, at doi:https://doi.org/10.1016/j.apcatb.2019.05.042.

References

[1] L. Qin, G. Zeng, C. Lai, D. Huang, P. Xu, C. Zhang, M. Cheng, X. Liu, S. Liu, B. Li, H. Yi, Coord. Chem. Rev. 359 (2018) 1–31.
[2] K. He, Z. Zeng, A. Chen, G. Zeng, R. Xiao, P. Xu, Z. Huang, J. Shi, L. Hu, G. Chen, Small 14 (2018) 1800871.
[3] L. Qin, G. Zeng, C. Lai, D. Huang, C. Zhang, P. Xu, T. Hu, X. Liu, M. Cheng, Y. Liu, L. Hu, Y. Zhou, Sens. Actuators B-Chem. 243 (2017) 946–954.
[4] P. Ilgin, O. Ozay, H. Ozay, Appl. Catal. B: Environ. 241 (2019) 415–423.
[5] B. Li, C. Lai, G. Zeng, L. Qin, H. Yi, D. Huang, C. Zhou, X. Liu, M. Cheng, P. Xu, C. Zhang, F. Huang, S. Liu, ACS Appl. Mater. Inter. 10 (2018) 18824–18836.
[6] L. Zhang, J. Zhang, G. Zeng, H. Dong, Y. Chen, C. Huang, Y. Zhu, R. Xu, Y. Cheng, K. Hou, Bioresour. Technol. Rep. 261 (2018) 10–18.
[7] H. Mou, C. Song, Y. Zhou, B. Zhang, D. Wang, Appl. Catal. B: Environ. 221 (2018) 565–573.
[8] L. Wang, J. Zhang, H. Wang, Y. Shao, X. Liu, Y.-Q. Wang, J.P. Lewis, F.-S. Xiao, ACS Catal. 6 (2016) 4110–4116.
[9] C. Lai, G.-M. Zeng, D.-L. Huang, M.-H. Zhao, Z. Wei, C. Huang, P. Xu, N.-J. Li, C. Zhang, M. Chen, X. Li, M. Lai, Y. He, Spectrochim. Acta A. 132 (2014) 369–374.
[10] Z. Yan, L. Fu, X. Zuo, H. Yang, Appl. Catal. B: Environ. 226 (2018) 23–30.
[11] C. Lai, M.-M. Wang, G.-M. Zeng, Y.-G. Liu, D.-L. Huang, C. Zhang, R.-Z. Wang, P. Xu, M. Cheng, C. Huang, Appl. Surf. Sci. 390 (2016) 368–376.
[12] W. Xiong, Z. Zeng, X. Li, G. Zeng, R. Xiao, Z. Yang, Y. Zhou, C. Zhang, M. Cheng, L. Hu, Chemosphere 210 (2018) 1061–1069.
[13] H. Yi, M. Yan, D. Huang, G. Zeng, C. Lai, M. Li, X. Huo, L. Qin, S. Liu, X. Liu, B. Li, H. Wang, M. Shen, Y. Fu, X. Guo, Appl. Catal. B: Environ. 250 (2019) 52–62.
[14] Y. Fu, T. Huang, B. Jia, J. Zhu, X. Wang, Appl. Catal. B: Environ. 202 (2017) 430–437.
[15] A.D. Quast, M. Bornstein, B.J. Greydanus, I. Zharov, J.S. Shumaker-Parry, ACS Catal. 6 (2016) 4729–4738.
[16] J.-L. Gong, B. Wang, G.-M. Zeng, C.-P. Yang, C.-G. Niu, Q.-Y. Niu, W.-J. Zhou, Y. Liang, J. Hazard. Mater. 164 (2009) 1517–1522.
[17] X. Du, C. Li, L. Zhao, J. Zhang, L. Gao, J. Sheng, Y. Yi, J. Chen, G. Zeng, Appl. Catal. B: Environ. 232 (2018) 37–48.
[18] J. Sheng, C. Li, L. Zhao, X. Du, L. Gao, G. Zeng, Fuel 197 (2017) 397–406.
[19] K. Tong, A. Lin, G. Ji, D. Wang, X. Wang, J. Hazard. Mater. 308 (2016) 113–119.
[20] Y. Xie, C. Li, L. Zhao, J. Zhang, G. Zeng, X. Zhang, W. Zhang, S. Tao, Appl. Surf. Sci. 333 (2015) 59–67.

[21] Z. Li, L. Wu, H. Liu, H. Lan, J. Qu, Chem. Eng. J. 228 (2013) 925–934.
[22] D. Huang, R. Deng, J. Wan, G. Zeng, W. Xue, X. Wen, C. Zhou, L. Hu, X. Liu, P. Xu, J. Hazard. Mater. 348 (2018) 109–116.
[23] S. Wang, Q. Zhao, H. Wei, J.Q. Wang, M. Cho, H.S. Cho, O. Terasaki, Y. Wan, J. Am. Chem. Soc. 135 (2013) 11849–11860.
[24] C. Zhou, C. Lai, C. Zhang, G. Zeng, D. Huang, M. Cheng, L. Hu, W. Xiong, M. Chen, J. Wang, Y. Yang, L. Jiang, Appl. Catal. B: Environ. 238 (2018) 6–18.
[25] M.-Y. Kuo, C.-F. Hsiao, Y.-H. Chiu, T.-H. Lai, M.-J. Fang, J.-Y. Wu, J.-W. Chen, C.-L. Wu, K.-H. Wei, H.-C. Lin, Y.-J. Hsu, Appl. Catal. B: Environ. 242 (2019) 499–506.
[26] C. Lai, M. Zhang, B. Li, D. Huang, G. Zeng, L. Qin, X. Liu, H. Yi, M. Cheng, L. Li, Z. Chen, L. Chen, Chem. Eng. J. 358 (2019) 891–902.
[27] P. Xu, G.M. Zeng, D.L. Huang, C.L. Feng, S. Hu, M.H. Zhao, C. Lai, Z. Wei, C. Huang, G.X. Xie, Z.F. Liu, Sci. Total Environ. 424 (2012) 1–10.
[28] C. Lai, X. Liu, L. Qin, C. Zhang, G. Zeng, D. Huang, M. Cheng, P. Xu, H. Yi, D. Huang, Microchim. Acta. 184 (2017) 2097–2105.
[29] E. Pashai, G. Najafpour Darzi, M. Jahanshahi, F. Yazdian, M. Rahimnejad, Int. J. Biol. Macromol. 108 (2018) 250–258.
[30] T. Parandhaman, N. Pentela, B. Ramalingam, D. Samanta, S.K. Das, ACS Sustain. Chem. Eng. 5 (2016) 489–501.
[31] C. Lai, S. Liu, C. Zhang, G. Zeng, D. Huang, L. Qin, X. Liu, H. Yi, R. Wang, F. Huang, B. Li, T. Hu, ACS Sens. 3 (2018) 2566–2573.
[32] R. Das, V.S. Sypu, H.K. Paumo, M. Bhaumik, V. Maharaj, A. Maity, Appl. Catal. B: Environ. 244 (2019) 546–558.
[33] C. Lai, B. Li, M. Chen, G. Zeng, D. Huang, L. Qin, X. Liu, M. Cheng, J. Wan, C. Du, F. Huang, S. Liu, H. Yi, Int. J. Hydrogen Energ. 43 (2018) 1749–1757.
[34] S. Giri, R. Das, C. van der Westhuyzen, A. Maity, Appl. Catal. B: Environ. 209 (2017) 669–678.
[35] S.M. Alshehri, T. Almuqati, N. Almuqati, E. Al-Farraj, N. Alhokbany, T. Ahamad, Carbohyd. Polym. 151 (2016) 135–143.
[36] S. Nellaiappan, A.S. Kumar, S. Nisha, K. Chandrasekara Pillai, Electrochim. Acta 249 (2017) 227–240.
[37] L. Qin, D. Huang, P. Xu, G. Zeng, C. Lai, Y. Fu, H. Yi, B. Li, C. Zhang, M. Cheng, C. Zhou, X. Wen, J. Colloid Interf. Sci. 534 (2019) 357–369.
[38] Y. Huang, Y. Fang, L. Chen, A. Lu, L. Zhang, Chem. Eng. J. 315 (2017) 573–582.
[39] C. Zhou, C. Lai, D. Huang, G. Zeng, C. Zhang, M. Cheng, L. Hu, J. Wan, W. Xiong, M. Wen, X. Wen, L. Qin, Appl. Catal. B: Environ. 220 (2018) 202–210.
[40] J. Zhang, G. Chen, M. Chaker, F. Rosei, D. Ma, Appl. Catal. B: Environ. 132-133 (2013) 107–115.
[41] R. Si, M. Flytzani-Stephanopoulos, Angew. Chem. 120 (2008) 2926–2929.
[42] J. Zhao, B. Wang, Y. Yue, S. Di, Y. Zhai, H. He, G. Sheng, H. Lai, Y. Zhu, L. Guo, X. Li, J. Catal. 365 (2018) 153–162.
[43] P.R. Shukla, S. Wang, H. Sun, H.M. Ang, M. Tadé, Appl. Catal. B: Environ. 100 (2010) 529–534.
[44] E. Truszkiewicz, W. Raróg-Pilecka, K. Schmidt-Szałowski, S. Jodzis, E. Wilczkowska, D. Łomot, Z. Kaszkur, Z. Karpiński, Z. Kowalczyk, J. Catal. 265 (2009) 181–190.
[45] B. Wang, B. Chen, Y. Sun, H. Xiao, X. Xu, M. Fu, J. Wu, L. Chen, D. Ye, Appl. Catal. B: Environ. 238 (2018) 328–338.
[46] T.B. Nguyen, C. Huang, R.-a. Doong, Appl. Catal. B: Environ. 240 (2019) 337–347.
[47] E. Menumerov, R.A. Hughes, S. Neretina, Nano Lett. 16 (2016) 7791–7797.
[48] J.-h. Sim, T. Kim, Acs Appl. Energy Mater. 160 (2015) 999–1006.
[49] V.K. Gupta, N. Atar, M.L. Yola, Z. Ustundag, L. Uzun, Water Res. 48 (2014) 210–217.
[50] X. Zhou, C. Lai, D. Huang, G. Zeng, L. Chen, L. Qin, P. Xu, M. Cheng, C. Huang, C. Zhang, J. Hazard. Mater. 346 (2018) 113–123.
[51] S. Wunder, F. Polzer, Y. Lu, Y. Mei, M. Ballauff, J. Phys. Chem. C 114 (2010) 8814–8820.
[52] M.A. Koklioti, T. Skaltsas, Y. Sato, K. Suenaga, A. Stergiou, N. Tagmatarchis, Nanoscale 9 (2017) 9685–9692.
[53] K. He, G. Chen, G. Zeng, A. Chen, Z. Huang, J. Shi, T. Huang, M. Peng, L. Hu, Appl. Catal. B: Environ. 228 (2018) 19–28.
[54] W. Zhong, T. Jiang, Y. Dang, J. He, S.-Y. Chen, C.-H. Kuo, D. Kriz, Y. Meng, A.G. Meguerdichian, S.L. Suib, Appl. Catal. A Gen. 549 (2018) 302–309.
[55] F. Li, L. Zhang, C. Hu, X. Xing, B. Yan, Y. Gao, L. Zhou, Appl. Catal. B: Environ. 240 (2019) 132–140.
[56] M. Bhaumik, R.I. McCrindle, A. Maity, Chem. Eng. J. 260 (2015) 716–729.